Adsorption of the Color Pollutant onto NiO Nanoparticles Prepared by a New Green Method

Omar Sadiq Ali *, Dunya Edan AL-Mammar
Department of Chemistry, College of Science, University of Baghdad, Baghdad, Iraq

Received: 15/2/2023 Accepted: 22/4/2023 Published: 30/4/2024

Abstract

Green synthesis methods have emerged as favorable techniques for the synthesis of nano-oxides due to their simplicity, cost-effectiveness, eco-friendliness, and non-toxicity. In this study, Nickel oxide nanoparticles (NiO-NPs) were synthesized using the aqueous extract of Laurus nobilis leaves as a natural capping agent. The synthesized NiO-NPs were employed as an adsorbent for the removal of Biebrich Scarlet (BS) dye from aqueous solution using adsorption technique. Comprehensive characterization of NiO-NPs was performed using various techniques such as atomic force microscopy (AFM), Fourier transform infrared (FTIR), X-ray diffraction (XRD), Brunauer-Emmett and Teller (BET) analysis, and scanning electron microscopy (SEM). Additionally, operational parameters including adsorbent weight, adsorption duration, temperature, pH value, and initial BS dye concentration were optimized for the adsorption process. Isotherm analysis indicated a better fit of the Langmuir model with equilibrium experimental data than the Freundlich model. The kinetic study revealed that the Pseudo-second-order (PSO) model was more suitable to represent the adsorption process compared to the Pseudo-first-order (PFO) kinetic model. Thermodynamic analysis encompassing the changes in Gibbs free energy (ΔG°), enthalpy (ΔH°), and entropy (ΔS°) unveiled that the adsorption of BS dye onto NiO-NPs was a spontaneous endothermic process with an increase in the randomness.

Keywords: Green synthesis; NiO-NPs; Adsorption technique; Biebrich Scarlet (BS)

امتزاز الملوث اللوني على دقائق NiO النانوية المحضرة بطريقة خضراء جديدة

عمر صادق علي * , دنيا عيدان المعمار

قسم الكيمياء, كلية العلوم, جامعة بغداد, بغداد, العراق

الخلاصة

ظهرت طرق التخليق الخضراء كتقنيات مواتية لتخليق اكاسيد النانو بسبب بساطتها, فعاليتها من حيث التكلفة, مراعاة البيئة وعدم سميتها. في هذه الدراسة, تم تخليق جسيمات أكسيد النيكل النانوية NiO-NPs باستخدام المستخلص المائي لأوراق نبات الغار كعامل للتحجيم. تم استخدام دقائق اوكسيد النيكل المخلقة كمادة مازه لإزالة صبغة الببرش القرمزية (BS) من المحاليل المائية باستخدام تقنية الامتزاز . تم اجراء توصيف كامل لـ NiO-NPs باستخدام تقيات مختلفة مثل مجهر القوة الذرية (AFM), طيف الاشعة تحت الحمراء (FTIR), حيود الاشعة السينية (XRD), تحليل برونر ايميت و تيلر (BET) والمسح المجهري الالكتروني (SEM). بالإضافة الى ذلك تم تحسين المعلمات التشغيلية لعملية الامتزاز المتضمنة وزن المادة المازة, فترة الامتزاز, درجة الحرارة, قيمة الاس الهيدروجيني والتركيز الابتدائي لصبغة الببرش القرمزية. أشار تحليل الإزاحة إلى أن نموذج لانغمير كان يلائم البيانات التجريبية للتوازن بشكل أفضل من نموذج فروندليش. كشفت الدراسة الحركية بأن إنموذج

* Email: omar.ali2105m@sc.uobaghdad.edu.iq

المرتبة الثانية الكاذبة (PSO) كان اكثر ملائمة لتمثيل عملية الامتزاز بالمقارنة مع الأنموذج الحركي المرتبة الاولى الكاذب (PFO). كشف التحليل الدينمي الذي يشمل التغير في طاقة كيس الحرة (ΔG^o), الانثالبي (ΔH^o) والإنتروبي (ΔS^o) ان امتزاز صبغة BS على NiO-NPs كان عملية ماصة للحرارة, تلقائية مع زيادة العشوائية .

1. Introduction

Pollution refers to the release of physical or chemical substances into the environment in quantities or ways that hinder the environment's ability to process them, leading to adverse effects on the ecosystem [1]. Since water is a vital component of life, its quality directly impacts human health. However, the rise of industrialization in recent times has resulted in severe contamination of surface water. Various industries, such as textile, paper, printing, and leather tanning, use synthetic dyes, many of which are toxic and even carcinogenic. Consequently, discharging these organic dyes into aquatic environments poses a significant risk to human health. Therefore, it is essential to remove dye contaminants from water [2]. Different techniques, such as adsorption, photodegradation, coagulation, and chemical oxidation, are used to remove organic dyes from wastewater. Among these techniques, adsorption is one of the most effective methods for eliminating dye due to its simplicity, low cost, and high efficiency [3].

A variety of substances, such as fly ash, zeolites, activated carbons, clay minerals, and polymers, have been used as adsorbents to remove dyes [4]. Most of these common adsorbents continue to have issues, such as slow adsorption kinetics, low selectivity, and low adsorption capacity. Therefore, using cutting-edge adsorbents is crucial to eliminating organic dyes from wastewater. Porous metal oxides have attracted a lot of interest for this use due to the advantages of quick diffusivities, great adsorption capacities, and large specific surface areas [5].

A significant and cutting-edge transition metal oxide, nickel oxide nanoparticles (NiO-NPs) are advantageous due to their high chemical and thermal stability, compatibility with the environment, and low cost. It is a solid, green substance with a molar mass of 74.692 g/mol. Numerous industries have used NiO-NPs frequently as catalysts, oxidizers, and drug carriers [6].

NiO-NPs have been produced using a variety of methods, including hydrothermal, sol-gel, thermal breakdown, and ball milling. Due to the fact that they generate stable nanoparticles that are inexpensive, straightforward, and biocompatible, green synthesis techniques are an alternative to chemical and physical methods [7].

The study produced NiO-NPs through a new eco-friendly approach, which involved utilizing the aqueous extract of Laurus nobilis leaves. These NiO-NPs were then utilized as an adsorbent for removing Biebrich scarlet dye from its water-based solution.

2. Materials and methods

2.1. Materials

All chemicals were of analytical grade and were employed without further purification. Nickel nitrate hexahydrate $Ni(NO_3)_2.6H_2O$ with purity 99% was supplied by Thomas Baker Co.,Ltd, Sodium hydroxide, pure ethanol, Biebrich Scarlet dye were purchased from BDH.

2.1.1. Adsorbate

Biebrich Scarlet (BS) dye or acid red 66, is anionic dye, its IUPAC name is sodium-6-(2-hydroxynaphthylazo)-3,4-azodibenzenesulfonate, and its chemical formula $C_{22}H_{14}N_4Na_2O_7S_2$. This dye is water soluble, molar mass is 556.48 g/mol, λ_{max} 505 nm and color index (C.I. number) is 26905 [8]. The chemical structure for this dye is shown in Figure 1.

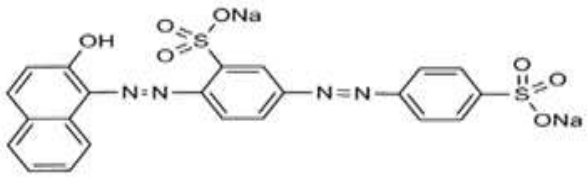

Figure 1- Chemical structure for BS dye

One gram of BS dye was dissolved in 1000 mL of distilled water to prepare 1000 ppm of the dye. The stock solution was then diluted to 10, 20, 30, 40, and 50 mg/L using distilled water. The absorbance of the solution is measured with a UV-Vis spectrophotometer.

2.1.2. Preparation leaf extract

To produce the NiO-NPs sample, Laurus nobilis leaf extract was utilized as a capping agent because of its various phytochemical compounds including Santamarine, Lauroxepine, and Zaluzanin. The leaves were cleaned by rinsing with water to eliminate any dust, and then cut into small pieces. To prepare the leaf extract, 5 grams of leaves were added to 100 mL of distilled water in a 250 mL conical flask. The mixture was stirred at 60°C for 20 minutes, filtered with Whatman No.1 filter paper, and stored at 4°C [9].

2.1.3. Preparation NiO-NPs

50 mL of distilled water was mixed with two grams of Ni $(NO_3)_2.6H_2O$ for 10 minutes, after which 50 mL of leaf extract was added. The mixture was then heated for 20 minutes at 60 °C. To bring the pH to 10, a few drops of 0.1M sodium hydroxide were added. The precipitate then appeared as a light green gel after being exposed to the air for 24 hours. It was then washed with distilled water to remove any unreacted particles, followed by ethanol alcohol, and the mixture was allowed to dry at 25 °C. In the end, it was heated for an hour at 110 C to create NiO-NPs as a powder.

2.2. Characterization

Atomic Force Microscopy (AFM) type (NaioAFM-2022-Switzerland**)** was used to describe a variety of nanoscale processes that need for accurate single molecules. Using a Panalytical X'pert Pro2021, the X-ray diffraction (XRD) pattern of nanoparticles is investigate with anode Cu kα(λ=0.154nm). Fourier transforms infrared spectroscopy (FTIR) measurement performed using a Shimadzu IR affinity (Japan) in the 4000-400 cm^{-1} region. Scanning electron microscopy (SEM) instrument type (Inspect f50-Fei Co.-Netherlands) is used to examine the surface morphology. Brunauer-Emmett and Teller (BET) analysis carried out using Micrometrics Gemini VII (Germany). UV-Vis spectrophotometer model (Shimadzu) was used to determine the maximum wavelength of the dye.

2.3 Adsorption experimental

Using the batch equilibrium method, adsorption experiments for the BS dye onto NiO-NPs were conducted. A specific amount of NiO-NPs sample was added to 25 mL of BS dye, the mixture was stirred on a shaker, and the mixture was centrifuged at 1000 rpm for 10 minutes to separate it. A UV-Vis spectrophotometer was used to measure the residual BS dye concentration. With the addition of a few drops of either 0.1 M HCl or 0.1 M NaOH, the impact of pH was investigated in the 2–10 pH range. Starting BS dye concentrations of 10–50 mg/L were used for the study. The adsorbent dosage for the kinetic study was 0.05 g/25 mL of dye solution at a concentration of 20 mg/L, with adsorption times of 5, 10, 20, 30, 40, 50, and 60 minutes. The following equations were used to determine the removal percentage (R%) for BS dye and the amount of adsorbed dye (qe) mg/g: [10]:

$$R\% = [\ (C_i - C_e) / C_i]_{\ x}\ 100 \quad (1)$$

$$q_e = (C_i - C_e)_{\ x}\ V/m \quad (2)$$

Where C_e (mg/L): the dye concentration at equilibrium, C_i (mg/L): the starting dye concentration, m (g): dosage of the adsorbent, and V (L): volume of the working solution.

3. Results and Discussion

3.1. Characterization

3.1.1. Atomic Force Microscopy (AFM)

Using the AFM technique, information was obtained regarding the volume, 3D characteristics, and average grain diameter. Figure 2 illustrates a typical surface and the cumulative distribution of granularity for the NiO-NPs sample. The findings indicate that the average diameter of the particles is 78.29 nm, while their average volume is 1.33 nm^3. These results suggest that the green biological procedures used in producing the sample had a significant impact on the NiO-NPs due to the presence of phytochemical compounds on their surface [11].

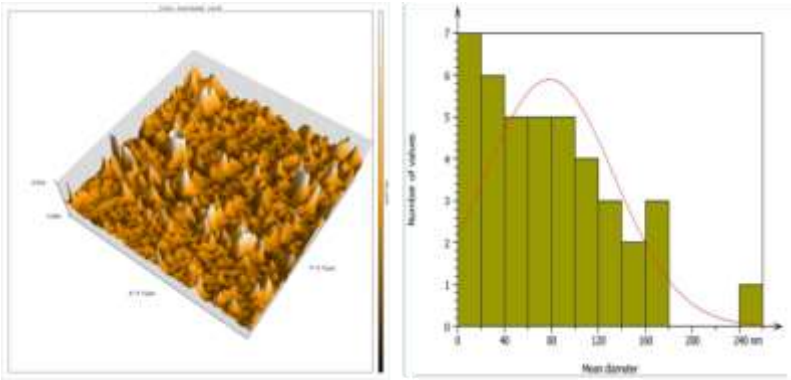

Figure 2- 3D AFM image and average mean diameter of NiO-NPs sample

3.1.2. Fourier transforms infrared spectroscopy (FTIR)

The FTIR spectrum for NiO-NPs sample is shown in Figure 3, the peaks 3641-3000 cm^{-1}, which is associated with the hydroxyl group(-OH) stretching vibration is due to the presence the water in sample [12]. It was observed that the location of the C−C and C−H groups at peaks

of 2825cm^{-1} and 2886 cm^{-1} respectively. The absorption peaks at 1780–1520 cm^{-1} match to the aromatic region include C=O and C=C groups. The peaks 1647–1624 cm^{-1} for C=C group for the aromatic rings, which are specific to the plant extract [13]. The bands 1492–1431 cm^{-1} seemed due to CH_2 group, while the peaks 1381–1300 cm^{-1}are indicated to CH_3 group, the peak at 1241 cm^{-1} is among others characteristic of the O=C-O-C ester bond present in the plant extract, while the absorption peaks appear at 1070 cm^{-1} belonged to the C-O bond stretch vibration of alcohols and carboxylic acid groups. Nitrate (NO^{3-}) peak were observed at 833 cm^{-1} [12, 14]. The peak at 671 cm^{-1} is related to the Ni-O-H stretching bond, whereas the other peaks (536-412 cm^{-1}) are connected with NiO bending vibrations [15].

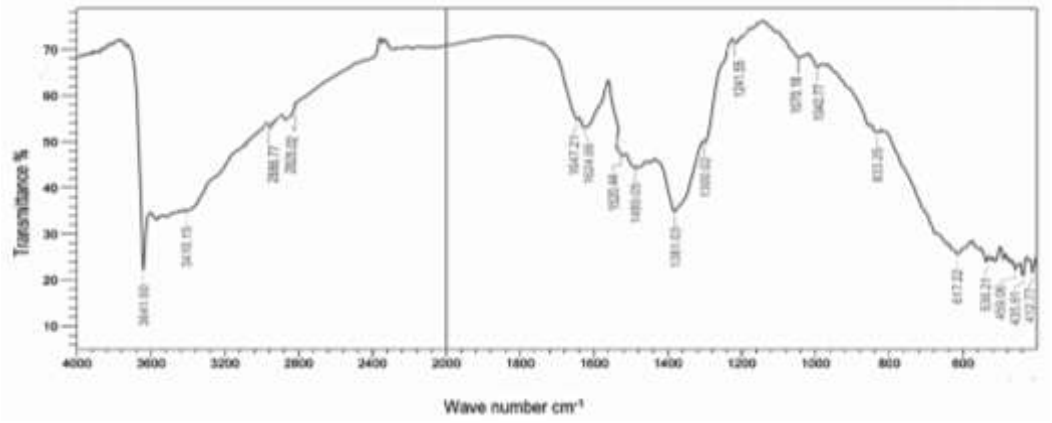

Figure 3- FTIR transmission for NiO−NPs

3.1.3. X-ray diffraction (XRD)

The XRD patterns for NiO-NPs are shown in Figure4. The peaks were observed at positions 37.08˚, 43.16˚, 62.14˚, 75.37˚ and 79.22˚ along with the rhombohedral cubic crystal structures at 2θº, while the WHFM values 0.205, 0.341, 0.273, 0.410 and 0.333 were corresponding to the same Miller indices 111, 200, 220, 311 and 222 respectively and the reference cards (JCPDS card No. 00-022-1189). The value of average crystal size (D) for sample was calculated using X'Pert High Score software is found to be 20.10 nm [16].

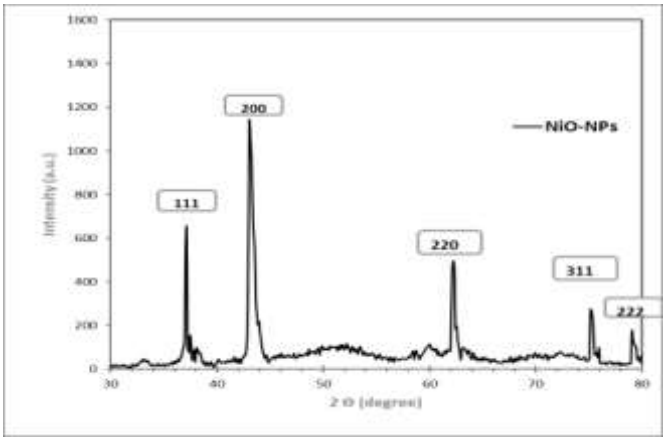

Figure 4- XRD Spectra of NiO-NPs sample

3.1.4. Scanning Electron Microscope (SEM)

SEM analysis is used to look at surface morphology, which includes nanoparticle distribution, size, and shape. The NiO-NPs sample's SEM image is depicted in Figure 5. The biosynthesised NiO-NPs were found to have a cubical morphology and to aggregate into more spherical, irregular, and geometric shapes of various sizes. Using the IMAGE J program, the particle sizes for NiO-NPs were calculated and found to be 25.73 nm. When phytochemicals are present on a particle's surface, their size is reduced and they become nanosized, which increases the porosity of their surface. These findings are in agreement with the research by Rashid I. et al. [17].

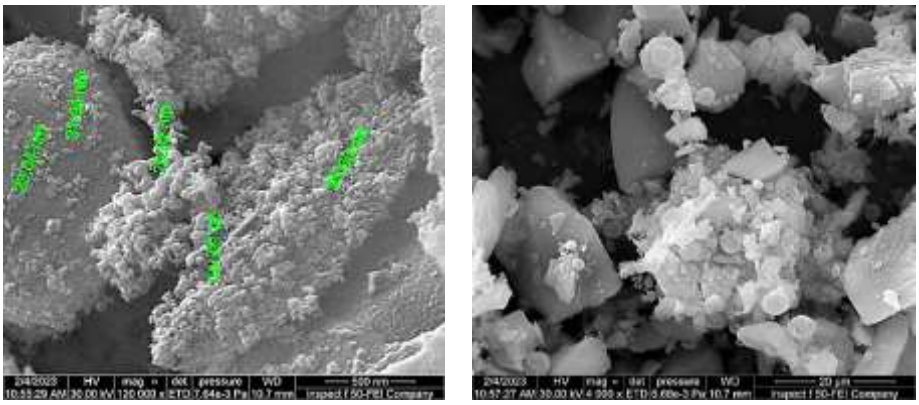

Figure 5- SEM images for the NiO-NPs sample

3.1.5. Brunauer–Emmett–Teller (BET) analysis

Based on the surface area and porosity data, the adsorption capacity and behaviour of the synthesized NiO-NPs were predicted [18]. The N_2 gas adsorption-desorption isotherm for NiO-NPs was illustrate in Figure 6. The specific surface area as calculated by BET method is found to be 66.415 m^2/g, the mean pore diameter is 20.679 nm and total pore volume is 0.1886 $cm^3.g^{-1}$. The value of pore size distribution that calculated from Barrett-Joyner-Halenda (BJH) method are found to be 8.21 nm.

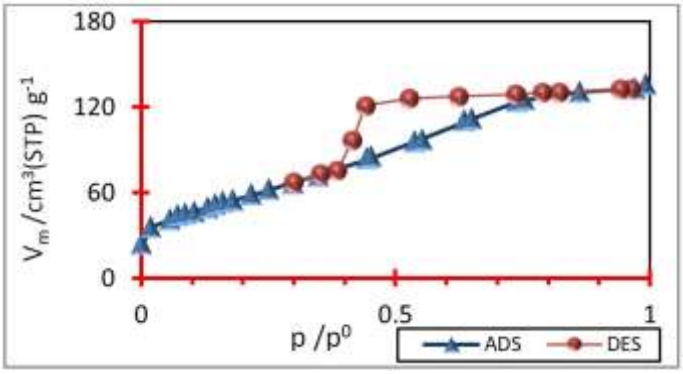

Figure 6- N_2 gas adsorption-desorption isotherm for NiO-NPs sample at 77 K.

3.2 Optimization study for the adsorption conditions

3.2.1. The influence of starting dye concentration

Under carefully controlled circumstances, different concentrations of BS dye (10, 20, 30, 40, and 50 mg/L) were used to investigate how the adsorption process is affected by the dye's initial concentration (298 K, pH 7, NiO-NPs dose of 0.05 g, 60 minute adsorption period, and shaking speed of 150 rpm). Figure 7(a, b) shows that the amount of adsorbed dye (q_e) increases from 4.80 to 20.88 mg/g as the starting concentration of BS dye increases, while the removal percentage (R%) decreases from 96.09% to 81.71%. Saturation is reached at a lower dye concentration once the starting BS dye concentration occupies the adsorbent surface sites. As a result, adding more BS dye to a solution does not cause further adsorption and, in fact, decreases dye removal at higher concentrations (Figure 7-a) [19]. As seen in Figure 7-b, as the starting BS dye concentration rises, so does the amount of adsorbed dye q_e. This might be because there are few available sites per unit dye concentration at low starting BS concentrations, which causes sorption to become independent of starting concentration. However, as dye concentration rises, more BS molecules are made available per unit mass, resulting in a gradual filling of the binding sites and an increase in qe values [20].

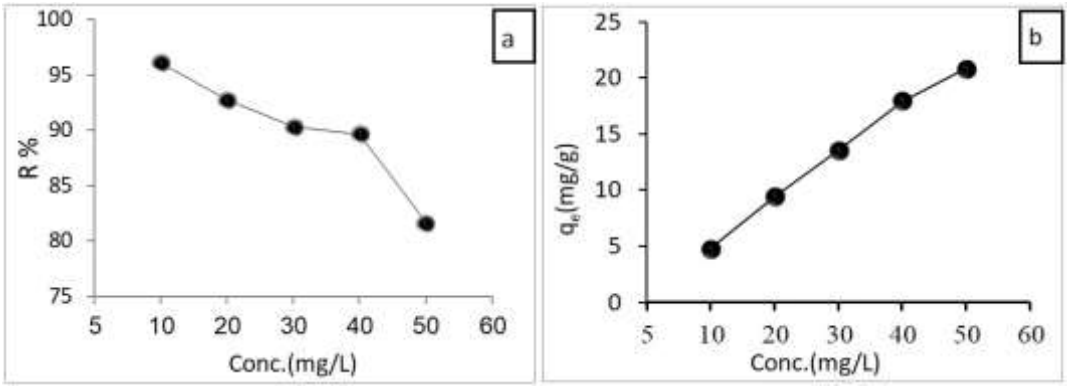

Figure 7- Influence starting BS dye concentration as a function of (a) Removal percentage (R%) (b) Amount of adsorbed dye(q_e)

3.2.2. The influence of NiO−NPs weight

Using 0.01, 0.03, 0.05, 0.07, 0.09, and 0.1 g of adsorbent, the effect of NiO-NPs weight on the removal percentage of BS dye was investigated. The experiment's other requirements were an initial BS dye concentration of 10 mg/L, a 40-minute adsorption period, and a pH of 7. The influence of the weight of NiO-NPs on the percentage of BS dye removal is shown in Figure 8. This graph shows that the value of R% increased from 60.54% to 96.72% as the weight of NiO-NPs increased. This increase is related to increasing the surface area of the adsorbent and the available adsorption sites [21]. According to the obtained result, 0.05 g was choosen as optimum weight for further experiments**.** Our results agree with Al-Mammar D., et al [22]

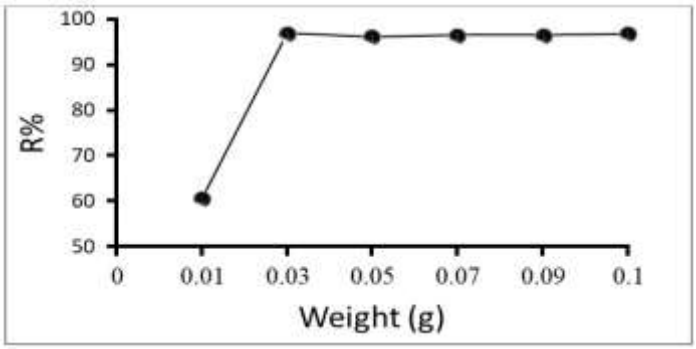

Figure 8- The influence of NiO-NPs weight on the R% of BS dye adsorption onto NiO-NPs sample.

3.2.3. The influence of adsorption period

The influence of adsorption period on the removal percentage for 10 mg/L BS dye was studied by changing the adsorption period from 10 to 60 minutes at 298 K, pH equals to 7 and NiO-NPs dosage is 0.05 g/25 mL. Figure 9 shows the influence of adsorption time on the removal percentage of BS dye. It can be observed that the value of R% suddenly increases at the time of 10 minutes and then it becomes almost steady at the time of 50 minutes. This may be attributed to availability of empty adsorption sites on the NiO-NPs surfaces, followed by a slight increases until the time reached the equilibrium [23]. So the optimum chosen time was 40 minutes.

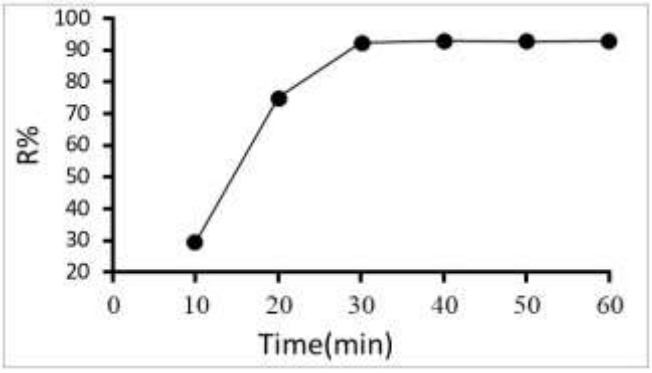

Figure 9- Influence of adsorption time on the removal percentage of BS dye using NiO-NPs sample.

3.2.4. The influence of temperature

The effect of temperature on the percentage removal of BS dye was investigated by varying the temperature from 293 to 318 K under optimal operating conditions: starting BS dye concentration of 10 mg/L, NiO-NPs dose of 0.05 g/25 mL, an adsorption period of 40 minutes, and a pH of 7. The findings are presented in Figure 10, which indicates that the percentage removal (R%) increases as the temperature rises. This suggests that the adsorption of BS dye onto NiO-NPs is endothermic and may be attributed to the sorption process [24].

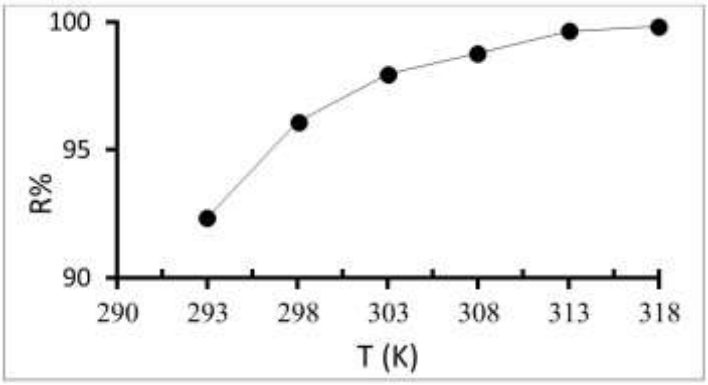

Figure 10- Influence of temperature on removal efficiency for BS dye adsorption onto NiO−NPs sample.

3.2.5. The influence of initial pH

The influence of pH on the R% was investigated by variation it between 2.2 and 10.3 at 298 K, BS dye concentration was 10 mg/L, adsorbent dosage of 0.05 g/ 25 mL and adsorption period was 40 minutes. Figure 11 shows the influence of pH on the removal percentage for BS dye using NiO-NPs. This Figure exhibit that the values of R% decreased from 99.6% to 84.5% with increasing in the pH values. At lower pH, the adsorption of the anionic dye can be promoted under acidic conditions, where the positive charge density on the adsorbent surface is a great. So, due to the electrostatic attraction between positively charged surface and negatively charge of BS dye, higher values for removal will be established, while at higher pH values, there are increasing in the negatively charged sites related to the presence OH^- ions that causes electrostatic repulsion as seen in Eqs. 3, 4 [25]:

$$Ni{-}OH + H^+ \longrightarrow NiOH_2^+ \quad (3)$$

$$Ni{-}OH + OH^- \longrightarrow Ni{-}O^- + H_2O \quad (4)$$

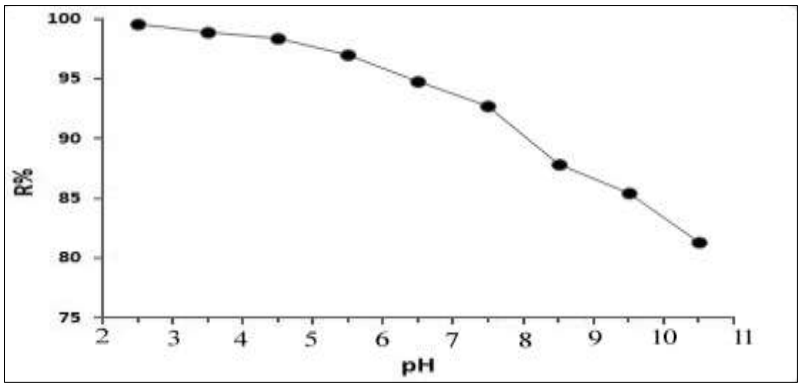

Figure 11- Impact of pH solution on the removal percentage of BS dye using NiO-NPs sample

3.3 Adsorption isotherm models

3.3.1 Langmuir isotherm

According to this model, the adsorption surface layer was uniform with identical sites for all adsorbate molecules and there is no interaction exist between molecules adsorbing on the specific places. Additionally, it is assumed that a signal adsorbate molecule can occupy an

active site leading to a single molecule as the adsorption layer thickness. The linear equation of this model expressed as [26]:

$$\frac{C_e}{q_t} = \frac{1}{K_L \,.\, Q_m} + \frac{C_e}{Q_m} \tag{5}$$

Where C_e is the dye concentration at equilibrium (mg/L), q_e refers to the equilibrium amount of the substance adsorbed per gram of the adsorbent (mg/g), Q_m is the maximum monolayer coverage (mg/g), and K_L is the Langmuir isotherm constant (L/mg) [27]. The values of K_L and Q_m are estimated from the linear plot between C_e/q_e against C_e (Figure 12a). The effectiveness of adsorption was calculated using the dimensionless constant or separation factor R_s which was estimated using the following equation [28].

$$R_s = \frac{1}{1+K_L.C_i} \tag{6}$$

Where C_i is the starting BS dye concentration $mg.L^{-1}$. The values of R_s specifies the adsorption was irreversible R=0, favourable ($0 < R_S < 1$), linear $R_s=1$ or unfavourable $R_s > 1$. The values of K_L, Q_m and R_s are listed in Table 1. From the values of R_s it can be noticed that these values between 0 and 1 ($0 < R_S < 1$) which indicates that the adsorption of BS dye onto NiO-NPs favourable [29].

3.3.2 Freundlich isotherm

The Freundlich linear equation can be written as [30]:

$$\ln q_e = \ln k_{fr} + \frac{1}{n_f} \ln C_e \tag{7}$$

Where k_{fr} is Freundlich constant related to the adsorption capacity $(mg/g\ (L/mg)^{-1/n})$ and n_f is the adsorption intensity, these values were estimated from the intercept and slope of linear relation between ln q_e and ln C_e Figure 12(b). The obtained values are shown in Table 1. It can be seen that the values of $1/n_f < 1$, indicating that the sorption of BS dye onto NiO-NPs is favorable. According to values of correlation coefficient R^2 for the both models, it can be predicted that the experimental data are well described by Langmuir models. Our results agree with AL-Shammari N., et al [31].

Table 1- Adsorption isotherm models constants.

Temp (K)	Langmuir isotherm				Freundlich isotherm		
	K_L (L/mg)	Rs	Q_m (mg/g)	R^2	n_f	K_{fr} $(mg/g(L/mg)^{-1/n})$	R^2
293	0.2615	0.2766	26.156	0.9990	1.72359	5.9072	0.9548
298	0.5375	0.1569	25.062	0.9949	2.05206	8.3131	0.9747
303	0.9177	0.0983	24.544	0.9956	2.4102	10.108	0.9809
308	1.0864	0.0777	26.075	0.9893	2.58199	11.521	0.9832
313	1.1040	0.0665	27.297	0.9906	2.53702	12.604	0.9883
318	1.1283	0.0493	27.943	0.9877	2.69665	14.351	0.9869

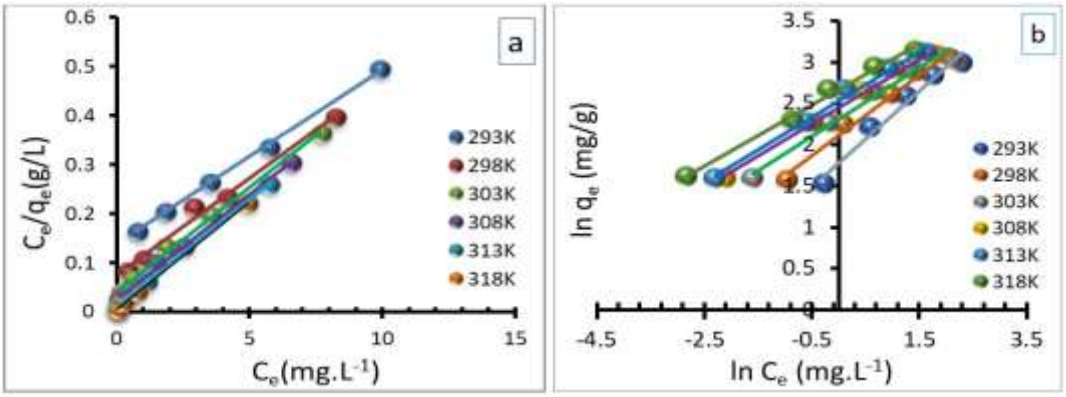

Figure 12- Adsorption isotherm plots for (a) Langmuir isotherm (b) Freundlich isotherm

3.4 Adsorption Thermodynamics

Thermodynamic parameters values are calculated using the following equations [32]:

$$\Delta G^{o} = -\,R\,T\,\ln K_{eq} \tag{8}$$

$$K_{eq} = q_e / C_e \tag{9}$$

$$\Delta G^{o} = \Delta H^{o} - T\,\Delta S^{o} \tag{10}$$

Where C_i and C_e (mg/L) are the starting and equilibrium concentrations of the BS dye respectively, K_{eq}: equilibrium constant for the adsorption process. V: Adsorbate volume (L), m: adsorbent dose (g), T(K): absolute temperature and R: the universal gas constant (8.314 J.mol/K). According to the Van't Hoff equation [33]:

$$\ln K_{eq} = -\frac{\Delta H^{\circ}}{R\,T} + \frac{\Delta S^{\circ}}{R} \tag{11}$$

The values of ΔH^{o} and ΔS^{o} are obtained from the slope and intercept of the plot between the values of ln K_{qe} against 1/T (Figure 13). The values are reported in Table 2. Adsorption process was assumed to be spontaneous based on the negative values for the change in the Gibbs free energy ΔG^{o} at the specified temperature, however the positive values for ΔH° suggested that the process was endothermic. This may be attributed to the occurrence of the sorption process, which includes both adsorption and absorption. Additionally, the positive ΔS^{o} values, indicates that the degrees of randomness are nearly increased at the solid-liquid interface during the adsorption of BS dye onto NiO-NPs [34].

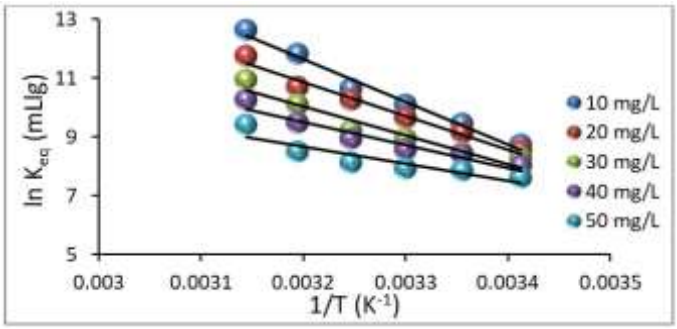

Figure 13- Van't Hoff plot for the adsorption of BS dye onto NiO−NPs

Table 2- Thermodynamic parameters for the adsorption of BS dye onto NiO-NPs.

C_i mg/L	ΔH^o (kJ/mol)	ΔS^o (J/mol.K)	(-)ΔG^o (kJ/mol)					
			293K	298K	303K	308K	313K	318K
10	79.777	345.864	21.206	23.331	25.412	27.196	28.135	30.021
20	44.327	223.386	20.707	22.499	23.640	24.730	25.416	26.509
30	47.394	230.207	20.063	21.216	22.489	23.285	24.633	25.919
40	34.861	185.954	19.483	20.737	21.522	22.395	23.230	24.315
50	30.478	167.070	18.536	19.415	19.952	20.895	21.780	22.794

3.5 Adsorption Kinetics model

The pseudo-first order PFO (Lagergren equation) written as [35]:

$$\ln(q_e - q_t) = \ln q_e - k_1 .t \quad (12)$$

Where q_t, q_e are the amount adsorbed at time t and at equilibrium ($mg.g^{-1}$), respectively, k_1 is the PFO rate constant (min^{-1}) for the adsorption process and t is the time (min). The slopes and intercepts of the plots between ln (q_e-q_t) against t, Figure 14(a) was used to estimate the PFO rate constants k_1 and q_e. These values were summarized in Table 4. It is obvious from this data that there is no fitted an agreement between the values of $q_{e\,cal}$ and $q_{e\,exp}$, this suggested that this model is less suitable for describing the adsorption process. The pseudo-second order(PSO) kinetics equation expressed as [36] :

$$\frac{t}{q_t} = \frac{1}{K_2.q_e^2} + \frac{t}{q_e} \quad (13)$$

Where k_2 is the equilibrium rate constant for the PSO equation (g/mg.min). The values of k_2 and q_e can be estimated from the intercept and the slope of plots between t/q_t versus t as shown in Figure 14(b), these values are shown in Table 3. According to the obtained results, it is clear that the values of correlation coefficients R^2 for the PSO model was higher than PFO model, also there is a good agreement between the values of $q_{e\,exp}$ and $q_{e\,cal}$, so we can suggested that the PSO sorption mechanism is predominant.

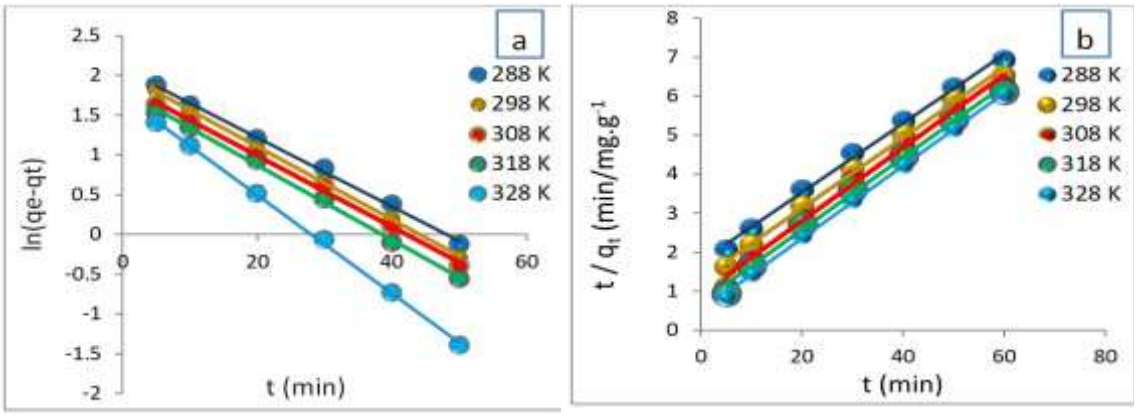

Figure 14- Adsorption kinetic plots for (a) PFO model (b) PSO model

Table 3- PFO and PSO kinetics data for the adsorption of BS dye onto NiO−NPs sample

PFO model					PSO model			
Temp. (K)	k_1 (1/min)	$q_{e\ cal}$ ($mg.g^{-1}$)	$q_{e\ exp}$ ($mg.g^{-1}$)	R^2	k_2 (g/mg.min)	$q_{e\ cal}$ ($mg.g^{-1}$)	$q_{e\ exp}$ ($mg.g^{-1}$)	R^2
288	0.0281	5.8229	9.0041	0.948	0.0092	9.8803	9.0041	0.9833
298	0.0342	5.5582	9.3160	0.9697	0.0116	10.112	9.3160	0.9861
308	0.0336	4.5834	9.4927	0.9838	0.0162	9.9967	9.4927	0.9925
318	0.0509	4.8346	9.8253	0.9813	0.0185	10.502	9.8253	0.9969
328	0.0536	4.5935	9.9397	0.9804	0.0231	10.489	9.9397	0.9983

4. Conclusions

NiO-NPs were synthesized using green methods with Laurus nobilis as the capping agent, resulting in a sample with high efficiency in removing BS dye through adsorption. Various techniques were used to confirm the synthesis of NiO-NPs. The Langmuir isotherm model provided a good fit for the adsorption of BS onto the NiO-NPs sample. Based on the thermodynamic parameters ΔH°, ΔS°, and ΔG°, it was found that the adsorption process is endothermic and occurs spontaneously. The results of the kinetics study indicated that PSO was the best model for representing the adsorption kinetics. In conclusion, the use of Laurus nobilis leaf extracts offered an easy and inexpensive method for synthesizing NiO-NPs.

References

[1] F. O. Ajibade *et al.*, "Chapter 25 - Environmental pollution and their socioeconomic impacts," in *Microbe Mediated Remediation of Environmental Contaminants*, A. Kumar, V. K. Singh, P. Singh, and V. K. Mishra Eds.: Woodhead Publishing, vpl. 12, pp. 321-354, 2021

[2] S. Wang, Y. Boyjoo, A. Choueib, and Z. H. Zhu, "Removal of dyes from aqueous solution using fly ash and red mud," *Water Research,* vol. 39, no. 1, pp. 129-138, 2005.

[3] R. A. Mohammed and D. E. Al-Mammar, "Using natural materials as corrosion inhibitors for carbon-steel on phosphoric acid medium," *Iraqi Journal of Science*, vol. 0, no. 0, pp. 40-45, 2019.

[4] Y. Qin, L. Wang, C. Zhao, D. Chen, Y. Ma, and W. Yang, "Ammonium-Functionalized Hollow Polymer Particles As a pH-Responsive Adsorbent for Selective Removal of Acid Dye," *ACS Applied Materials & Interfaces,* vol. 8, no. 26, pp. 16690-16698, 2016.

[5] M. A. Behnajady and S. Bimeghdar, "Synthesis of mesoporous NiO nanoparticles and their application in the adsorption of Cr(VI)," *Chemical Engineering Journal*, vol. 239, pp. 105-113, 2014.

[6] N. Cherkasov, "Liquid-phase adsorption: Common problems and how we could do better," *Journal of Molecular Liquids,* vol. 301, p. 112378, 2020.

[7] M. Aminuzzaman, L. P. Ying, W.-S. Goh, and A. Watanabe, "Green synthesis of zinc oxide nanoparticles using aqueous extract of Garcinia mangostana fruit pericarp and their photocatalytic activity," *Bulletin of Materials Science,* vol. 41, no. 2, p. 50, 2018.

[8] O. D. Onukwuli, I. A. Obiora-Okafo, and M. Omotioma, "Characterization And Colour Removal From An Aqueous Solution Using Bio-Coagulants: Response Surface Methodological Approach," *Journal of Chemical Technology & Metallurgy,* vol. 54, no. 1, 2019.

[9] N. Uchiyama *et al.*, "Trypanocidal terpenoids from Laurus nobilis L," *Chemical and pharmaceutical bulletin,* vol. 50, no. 11, pp. 1514-1516, 2002.

[10] S. A. Saed and D. E. AL-Mammar, "Influence of Acid Activation of a Mixture of Illite, Koalinite, and Chlorite Clays on the Adsorption of Methyl Violet 6B Dye," *Iraqi Journal of Science*, vol. 62, no. 6, pp. 1761–1778, Jul. 2021.

[11] A. Rheima, A. Anber, A. Shakir, A. Salah Hammed, and S. Hameed, "Novel method to synthesis nickel oxide nanoparticles for antibacterial activity," *Iranian Journal of Physics Research*, vol. 20, no. 3, pp. 51-55, 2020.
[12] Z. Sabouri, A. Akbari, H. A. Hosseini, and M. Darroudi, "Facile green synthesis of NiO nanoparticles and investigation of dye degradation and cytotoxicity effects," *Journal of Molecular Structure*, vol. 1173, pp. 931-936, 2018.
[13] A. M. Al-Wadi, D. E. Al-Mammar "Green Synthesis by Zygophyllum Coccineum Leaves Extract for Preparing ZnO Nanoparticles, and Characteristics Study," *Egypt. J. Chem*. Vol. 65, No.5, pp. 363-369, 2022.
[14] S. H. Alwan and H. A. Alshamsi, "In situ synthesis NiO/F-MWCNTs nanocomposite for adsorption of malachite green dye from polluted water," *Carbon Letters*, vol. 32, no. 4, pp. 1073-1084, 2022.
[15] X. H. Xia, J. P. Tu, J. Zhang, X. L. Wang, W. K. Zhang, and H. Huang, "Electrochromic properties of porous NiO thin films prepared by a chemical bath deposition," *Solar Energy Materials and Solar Cells*, vol. 92, no. 6, pp. 628-633, 2008.
[16] M. Darroudi, Z. Sabouri, R. K. Oskuee, A. K. Zak, H. Kargar, and M. H. N. Abd Hamid, "Sol–gel synthesis, characterization, and neurotoxicity effect of zinc oxide nanoparticles using gum tragacanth," *Ceramics International*, vol. 39, no. 8, pp. 9195-9199, 2013.
[17] I. Rashid, S. Salman, P. Kareem Mohammed, and Y. Mahdi, "Green Synthesis of Nickle Oxide Nanoparticles for Adsorption of Dyes," *Sains Malaysiana*, vol. 51, pp. 533-546, 2022.
[18] R. Chen, J. Yu, and W. Xiao, "Hierarchically porous MnO 2 microspheres with enhanced adsorption performance," *Journal of Materials Chemistry A*, vol. 1, no. 38, pp. 11682-11690, 2013.
[19] D. P. Samal, "Characterization of activated carbon and study of adsorption of methylene blue dye using activated carbon," 2014.
[20] R. A. Mohammed and D. E. Al-Mammar "Using tobacco leaves as adsorbent for the orange-G dye removal from its aqueous solutions," *J. Glob. Pharma Technol*, vol. 11, pp. 273-280, 2019.
[21] Z. Mi-Na, L. Xue-Pin, and S. Bi, "Adsorption of surfactants on chromium leather waste," *Journal-society of leather technologists and chemists*, vol. 90, no. 1, p. 1, 2006.
[22] R. A. Mohammed and D. E. Al-Mammar, "Application of Surfactant for Enhancing the Adsorption of Azo Dye Onto Buckthorn Tree Wood Surface," *Iraqi Journal of Science*, vol. 58, no. 4A, pp. 1780-1798, 2017.
[23] C. J. Pandian, R. Palanivel, and S. Dhananasekaran, "Green synthesis of nickel nanoparticles using Ocimum sanctum and their application in dye and pollutant adsorption," *Chinese Journal of Chemical Engineering*, vol. 23, no. 8, pp. 1307-1315, 2015.
[24] Z. Sabouri, A. Akbari, H. A. Hosseini, A. Hashemzadeh, and M. Darroudi, "Bio-based synthesized NiO nanoparticles and evaluation of their cellular toxicity and wastewater treatment effects," *Journal of Molecular Structure*, vol. 1191, pp. 101-109, 2019.
[25] Y. Zheng, B. Zhu, H. Chen, W. You, C. Jiang, and J. Yu, "Hierarchical flower-like nickel (II) oxide microspheres with high adsorption capacity of Congo red in water," *Journal of colloid and interface science*, vol. 504, pp. 688-696, 2017.
[26] P. Van Der Voort, K. Leus, and E. De Canck, *Introduction to Porous Materials*. John Wiley & Sons, 2019.
[27] N. Ayawei, A. N. Ebelegi, and D. Wankasi, "Modelling and interpretation of adsorption isotherms," *Journal of chemistry*, vol. 2017, 110-118, 2017.
[28] A. K. Abaas, D. E. Al-Mammar, and H. A. Abbas, "Equilibrium, Thermodynamic and Kinetic Study of the Adsorption of a New Mono Azo dye onto Natural Iraq Clay," *Journal of Global Pharma Technology* , vol. 10(5), pp. 102-109, 2009.
[29] K. P. Kuśmierek, L. Dąbek, and A. Świątkowski, "Comparative study on the adsorption kinetics and equilibrium of common water contaminants onto bentonite," *Desalination and Water Treatment*, vol. 186, pp. 373-381, 2020.
[30] K. A. Al-Saade, D. E. AL-Mammar, and H. N. AL-Ani, "Using Phragmites australis(Iraqi plant) to remove the Lead (II) Ions form Aqueous solution," *Baghdad Sci.J*, vol. 14, no. 1, pp. 0148, 2017.
[31] N. H. Al-Shammari and D. E. Al-Mammar, "Adsorption of Biebrich Scarlet Dye into Remains Chromium and Vegetable Tanned Leather as Adsorbents," *Iraqi Journal of Science*, vol. 63, no. 7, pp. 2814-2826, 2022.
[32] M. Mushtaq, H. N. Bhatti, M. Iqbal, and S. Noreen, "Eriobotrya japonica seed biocomposite efficiency for copper adsorption: Isotherms, kinetics, thermodynamic and desorption studies," *Journal of Environmental Management*, vol. 176, pp. 21-33, 2016.
[33] E. C. Lima, A. A. Gomes, and H. N. Tran, "Comparison of the nonlinear and linear forms of the van't Hoff equation for calculation of adsorption thermodynamic parameters (ΔS° and ΔH°)," *Journal of Molecular Liquids*, vol. 311, p. 113315, 2020.
[34] H. H. Kadhim and K. A. Saleh, "Removing Cobalt ions from Industrial Wastewater Using Chitosan," *Iraqi Journal of Science*, vol. 63, no. 8, pp. 3251-3263, 2022.

[35] A. A. Mizhir, H. S. Al-Lami, and A. A. Abdulwahid, "Kinetic, Isotherm, and Thermodynamic Study of Bismarck Brown Dye Adsorption onto Graphene Oxide and Graphene Oxide-Grafted-Poly (n-butyl methacrylate-co-methacrylic Acid)," *Baghdad Science Journal*, vol. 19, no. 1, p. 0132, 2022.

[36] N. H. AL-Shammari and D. E. AL-Mammar, "Equilibrium and kinetic modeling studies for the adsorption-desorption of methyl violet 10B onto leather waste," *Eurasian Chemical Communications*, vol. 4, no. 2, pp. 175-189, 2022.